Ageing processes of coil-coated materials: Temperature-controlled electrochemical impedance analysis

Nicolas Caussé, Pierre Bonin, Dominique Thierry, Nathalie Le Bozec, Aurélien Roggero, Nadine Pébère

Ageing processes of coil-coated materials: temperature-controlled electrochemical impedance analysis

Nicolas Caussé[1*], Pierre Bonin[1,2], Dominique Thierry[3], Nathalie Le Bozec[2]

Aurélien Roggero[4], Nadine Pébère[1*]

[1] *Physique des polymères CIRIMAT, Toulouse INP, Université Toulouse 3 Paul Sabatier, CNRS, Université de Toulouse, 4 allée Emile Monso - BP44362, 31030 Toulouse cedex 4 – France*

[2] *Institut de la Corrosion / French Corrosion Institute, 220 rue Pierre Rivoalon, 29200 Brest, France*

[3] *RISE Research Institutes of Sweden, Isafjordsgatan 28A, 16407 Kista, Sweden*

[4] *Université de Lyon, INSA Lyon, UCBL, CNRS, IMP UMR 5223, 69621 Villeurbanne, France*

KEYWORDS: organic coatings, barrier properties, water sorption, plasticization, blistering.

[*]Corresponding authors: nicolas.causse@ensiacet.fr (Nicolas Caussé) and nadine.pebere@ensiacet.fr (Nadine Pébère)

Abstract

In the present work, an industrial polyester coil-coated steel was characterized by electrochemical impedance spectroscopy (EIS) during immersion in a 0.5 M NaCl solution for different temperatures (30, 40, 50 and 60°C). The objective was to propose a methodology to follow the ageing of the coil-coated system, from the first stage of water uptake until the blistering appearance. Relevant parameters were extracted from the EIS diagrams to analyse ageing processes of the polymer and of the metal/polymer interface coil-coating. Water uptake was determined from the high-frequency part of the impedance diagrams using a linear rule of mixtures. By increasing the temperature, both the water uptake kinetics and the water content in the coating increased. The effect of water uptake on the physical structure of the coating (plasticization) was discussed through the analysis of a time constant corresponding to the dielectric manifestation of the polymer glass transition.

At 40, 50 and 60°C, appearance of corrosion was detected on the impedance spectra by a decrease, at low frequency, of the impedance modulus and of the phase angle. For 60°C, the corroded surface area as a function of time, was assessed from the EIS data analysis with adapted equivalent circuits. The corroded surface areas followed similar trend as blister surface areas determined from images analysis.

1. Introduction

Coil-coated materials used in the building industry generally provide excellent weathering and corrosion resistances. To evaluate or to compare coil-coatings performance, they need to be exposed outdoors for years. Therefore, it is important to develop methodologies to establish relationship between accelerated tests and field performance data [1,2]. In addition, there is still a lack of knowledge on blistering mechanisms and paint de-adhesion. Tendency of a paint system to blistering depends on several parameters, including surface contaminations, bulk properties of the polymer and interactions at the metal/polymer interface [3–5]. Water penetration is an initial step in the degradation process not only because water molecules interact both with the polymer matrix and the metal/polymer interface but also because water favours diffusion of ions from the environment to the interface [3,6–9]. Recently, Hoseinpoor *et al.* studied possible correlations between water permeability of free-standing paint films and blistering of the same systems in accelerated test and field exposures [10].

As a non-destructive technique, electrochemical impedance spectroscopy (EIS) could provide quantitative data on the performance of a coating [11–13]. EIS is a well-known technique for assessing water uptake during immersion in an electrolytic solution [14,15]. Precautions must be taken regarding the assumptions of the considered mixing law and the impedance values, particularly, the chosen frequency used for the calculation of the coating capacitance (or permittivity) [16–18]. Moreover, the nature of water as well as its interactions with the polymer matrix are rarely discussed. Equivalent electrical circuits have been extensively used to model the EIS response of diffusing or corroding systems [19–24]. For real systems, a distribution of electrical properties across the thickness or the volume was commonly noticed, resulting in deviations from simple capacitive or resistive behaviours. Due to the complexity of high-performance commercial coatings, the physical meaning of the extracted parameters is difficult to interpret. In particular, the dielectric response of the polymer remains

rarely studied, which limits the use of the technique for the understanding of the coating ageing phenomena.

In our recent work, an approach combining conventional impedance spectroscopy, dielectric spectroscopy (Cole-Cole analysis) and calorimetry (T_g measurements) was proposed to have a better knowledge of the initial steps which control the degradation process of a coil-coated steel [25]. The experiments were performed at room temperature and blistering was not observed, even after several months of immersion in a 0.5 M NaCl solution. However, the proposed approach allows an *in-situ* analysis of water uptake and of its effect on the physical structure of the organic coating.

The objective of the present study was to propose a methodology to evaluate and to describe the acceleration of the degradation processes (particularly, water uptake) of a coil-coating sample until the blistering appearance. Impedance measurements were performed at different temperatures ranging from 30 to 60°C and for various immersion times in a 0.5 M NaCl solution on the same coil-coating sample as in our previous study [25]. Relevant parameters were extracted from the diagrams to analyse the ageing processes of the coil-coated materials as a function of time and temperature. For 60°C, electrical equivalent circuits were used to follow the progression of corrosion/de-adhesion and then to compare the corroded surface area with the blistered surface area determined from optical observations.

2. Experimental

2.1. Coil-coated sample

The commercial coil-coated material was similar to that characterized in [25], composed of a galvanized steel (hot-dip galvanized steel with a zinc coating of 275 g/m²) on which a chromium-free primer and a top coat were deposited. Both polymer layers were based on polyester chemistry with a thickness of 5 µm and 20 µm for the primer and the topcoat, respectively. The primer was a polyester/melamine/epoxy system with a total pigment volume

concentration (PVC) of 18%, containing phosphates as inhibitive pigments. The topcoat was a polyester/melamine system with a total PVC of 22%. A surface treatment, based on Ti and Zr chemistry was applied before the primer deposition.

The coil-coating samples were dried for 16 h at 60°C (dry state) to start with similar reference conditions for all temperatures. It has been previously shown that "as-received" samples already contained water due to their storage period [25].

The glass transition temperature (T_g) of the dried samples has been measured at 25 ± 1°C (differential scanning calorimetry) [25]. Thus, all the impedance measurements were performed above T_g.

2.2. Electrochemical impedance measurements

Impedance measurements were carried out by using the Paint Cell Test (from Gamry). The coil-coated sample constituted the working electrode while a graphite rod acted as both counter and pseudo reference electrodes (two-electrode configuration) [26]. This configuration allows the frequency range to be increased to 1 MHz. The cell was filled with a 0.5 M NaCl (from *Merk*) solution and placed in an oven to perform the experiments at 30, 40, 50 and 60°C. The surface area of the coil-coated material in contact with the electrolyte was 14.6 cm².

The impedance measurements were performed with a Gamry REF600 apparatus. The diagrams were obtained every 2 h for 72 h and then, once a day, over a frequency range of 1 MHz to 0.01 Hz with 8 points per decade. An additional series of experiments was performed at a single frequency value (1 MHz) every 6 s during the first hour. The diagrams were obtained with a 20 mV_{rms} sinusoidal voltage perturbation at a potential of 0 V versus the reference electrode. The repeatability was checked for three independent samples, as illustrated in Fig. 8.

2.3. Impedance data analysis

To access the water uptake and the relaxation time associated with the coating glass transition, the impedance data were converted in term of complex dielectric permittivity $\varepsilon^*(\omega) = \varepsilon'(\omega) + i\varepsilon''(\omega)$ thanks to equations 1, 2 and 3.

$$\varepsilon'(\omega) = \frac{-Z(\omega)''}{\omega C_v (Z'(\omega)^2 + Z''(\omega)^2)} \quad (1)$$

$$\varepsilon''(\omega) = \frac{Z(\omega)'}{\omega C_v (Z'(\omega)^2 + Z''(\omega)^2)} \quad (2)$$

$$\text{with } C_v = \frac{\varepsilon_v A}{l} \quad (3)$$

where $\varepsilon'(\omega)$ is the real and $\varepsilon''(\omega)$ the imaginary parts of permittivity, ω is the angular frequency and C_v the capacitance of the equivalent vacuum-filled (ε_v is the vacuum permittivity) parallel plate capacitor formed by two electrodes of area *A* (here, the area of the EIS cell) separated by the distance *l* (here, the coating thickness).

Water volume fraction, $\varphi(t)$, was determined by using permittivity values measured at 1 MHz and a linear rule of mixtures between the water and the coating (Eq. 4). Several works on different coatings have shown that this equation leads to better agreement with gravimetric measurements than the Brasher and Kingsbury equation [15,17].

$$\varphi(t) = \frac{\varepsilon'_f(t) - \varepsilon'_f(0)}{\varepsilon_{water} - \varepsilon'_f(0)} \quad (4)$$

Where $\varepsilon'_f(t)$ is the permittivity for each immersion time and $\varepsilon'_f(0)$ is obtained by extrapolation of the permittivity at t = 0 from the plot of $\varepsilon'_f(t)$ as a function of the square root of the immersion time. Water permittivity, ε_{water}, is a decreasing function of temperature. The equation proposed by Malmberg and Maryott [27] was used to calculate the water permittivity for the different temperatures and the values are reported in Table 1.

Table 1: Water permittivity at different temperatures calculated from the work of Malmberg and Maryott [27]

Temperature (°C)	30	40	50	60
ε_{water}	77	73	70	67

The relaxation time, τ, associated with the dielectric manifestation of the glass transition was extracted from the imaginary part of the permittivity (Eq. 2) for the different conditions (temperature and immersion time), following the methodology developed in previous works (see for example Fig. 6 and Fig. 7 in [25]).

2.4. Optical microscopy

For 60°C, the coil-coated sample was observed after different immersion times in the NaCl solution by optical microscopy with a Nikon MA200 and blistered surface areas were evaluated by Image J software.

3. Results

The presentation of the obtained results is divided into two parts. First, the effect of water uptake on the polymer plasticization was investigated by EIS as a function of temperature. Then, at 60°C, the corrosion process associated with blistering was analysed to follow the corroded surface area.

3.1. Water uptake acceleration

A comparison of the impedance spectra obtained at 30, 40, 50 and 60°C for different coil-coating samples after 24 h of immersion in the NaCl solution is shown in Fig. 1. It must be pointed out that after 24 h of immersion, independently of the temperature, there is no evidence of corrosion or blistering. When the temperature increases, the diagrams evolve from a pure capacitive behaviour (straight line) to a resistive behaviour at low frequency (constant

impedance modulus values), particularly at 60°C. Modifications are observed on the phase angle and additional time constants can be identified. In the absence of corrosion, and as previously shown, these time constants can be associated with dielectric relaxations (interfacial polarization or orientation polarization of permanent dipoles on the polymer chains [28]). The comparison of the diagrams in Fig. 1 emphasizes the significant effect of the electrolyte temperature on the coil-coated steel behaviour.

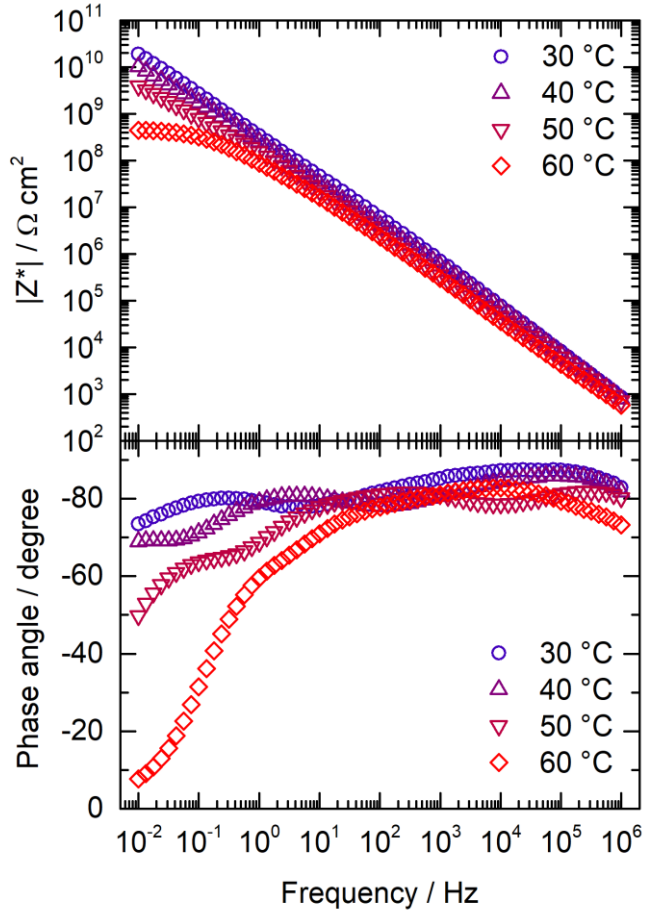

Fig. 1. Impedance diagrams (Bode plots) for the coil-coated samples after 24 h of immersion in a 0.5 M NaCl solution at different temperatures. The curves correspond to independent samples.

Impedance diagrams were acquired for the different temperatures during immersion in the NaCl solution. Some diagrams obtained at 40°C (from 25 to 528 h) are shown in Fig. 2. Between 25 and 240 h (Fig. 2a), the diagrams are almost unchanged. They present a capacitive behaviour on the whole frequency range. Two time constants are visible on the phase angle. The time constant at high frequency (around 10^2 Hz for 25 h of immersion) is attributed to the

signature of the dielectric manifestation of the glass transition, as already observed at ambient temperature [25]. This time constant shifts toward higher frequencies when the immersion time increases. Its variation with time and temperature will be discussed further in section 3.1.2. The second time constant at low frequency (around 0.1 Hz) is independent of the immersion time. It can be assigned to a Maxwell-Wagner-Sillars (MWS) type relaxation [28] and would correspond to interfacial charge accumulation such as primer/topcoat, primer/substrate and/or polymer/fillers interfaces. This time constant at low frequency will not be discussed further.

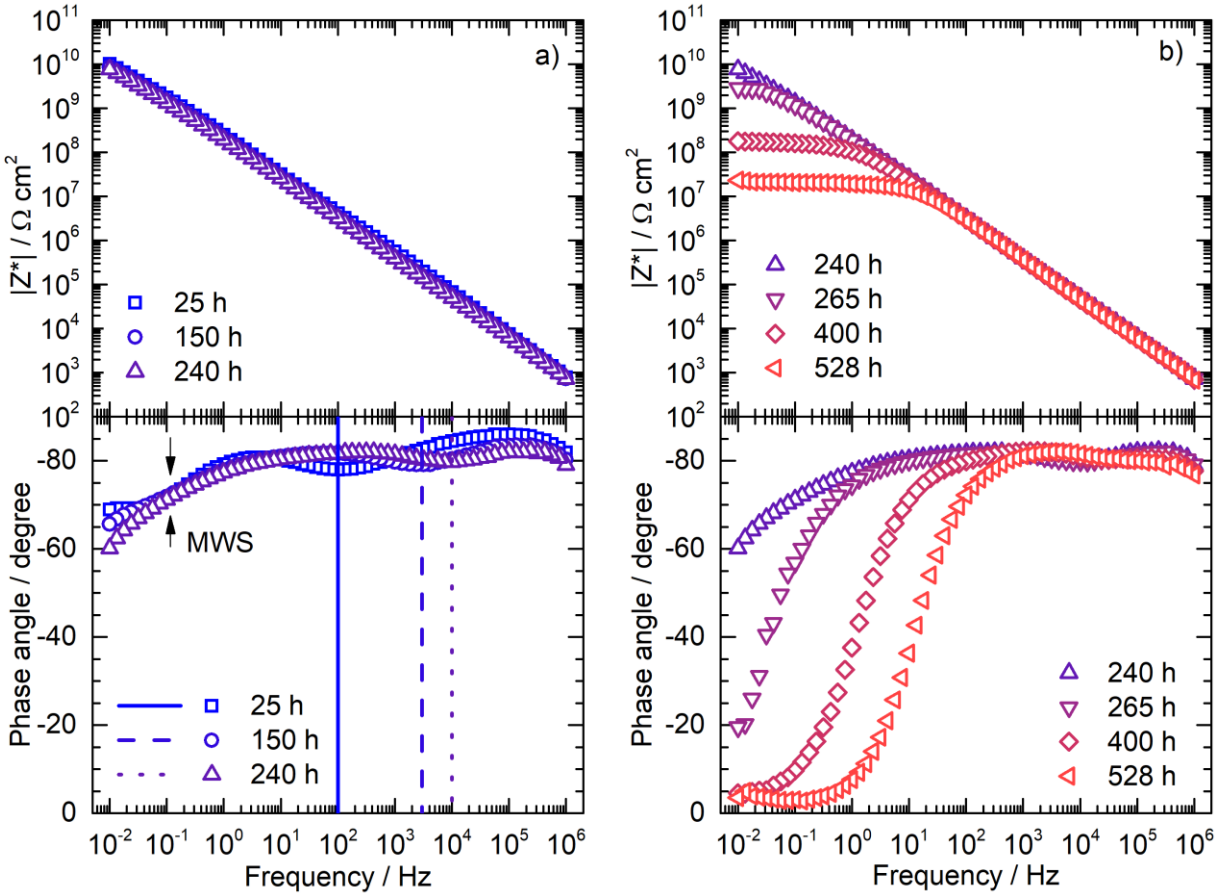

Fig. 2. Impedance diagrams (Bode plots) for the coil-coated sample obtained during immersion in a 0.5 M NaCl solution at 40°C: (a) 25 to 240 h and (b) 240 to 528 h. (MWS: Maxwell-Wagner-Sillars relaxation).

Between 240 and 528 h of immersion (Fig. 2b), a decrease of both the impedance modulus and the phase angle is observed at low frequency. The decrease of the impedance modulus is accompanied by the presence of a plateau increasingly pronounced. For the longest immersion

times, a third time constant starts to appear at very low frequency (below 0.1 Hz). The change in behaviour between the two types of diagrams (which appears for this sample between 240 and 265 h) is attributed to the onset of corrosion (electrochemical activity in relation with blistering phenomena). Then, the corroded surface areas (or the blisters areas) would increase with increasing immersion time.

Similar behaviours were observed for the different temperatures, with an acceleration of the ageing processes when the temperature increased. The variations of the two ageing parameters (water uptake and relaxation time associated with the dielectric manifestation) were followed over the immersion time in the NaCl solution and compared for the different temperatures. The results are presented below.

3.1.1. Dielectric manifestation of the glass transition

The relaxation time (τ) variations during immersion in the NaCl solution and for the different temperatures are reported in Fig. 3. First, it should be mentioned that for 50 and 60°C, the time constant shifted towards higher frequencies when the immersion time increased. It was outside the measured frequency range (> 1 MHz) after 100 h at 50°C and after 24 h at 60°C. In Fig. 3, a rapid decrease of the relaxation time is observed for short immersion times. This decrease is much faster when the temperature increases. When the immersion time increases, the decrease of τ is slower without stabilization, even for the longest immersion times (1300 h for 30°C). As previously discussed [25,29], these variations are linked to the water content within the coating and, as expected, τ decreases with increasing immersion time due to water plasticizing effect [30]. The strong decrease of τ over immersion time, going down five-six decades for the two highest temperatures, shows a significant rise of the plasticization.

Noteworthy is the fact that corrosion initiation (as it will be discussed later) is not detected on the relaxation time variation. This was indeed expected because the coating properties are independent of the corrosion phenomena.

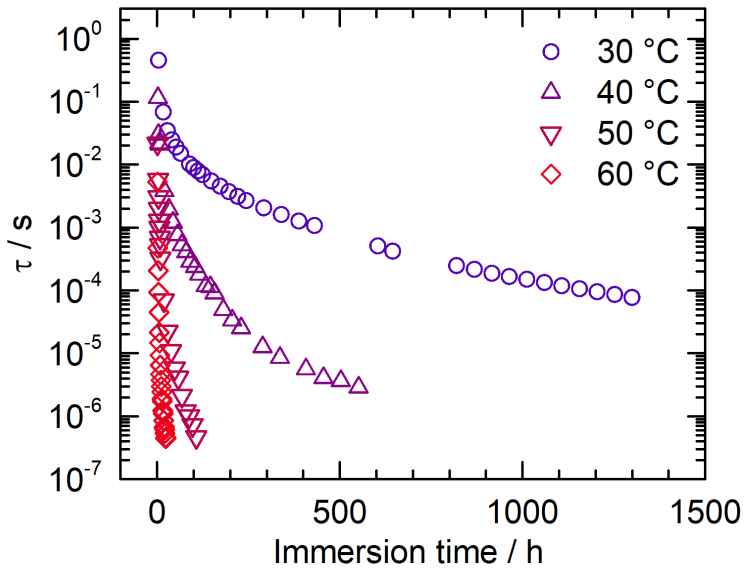

Fig. 3. Variation of the relaxation time (τ) of the dielectric manifestation of the glass transition as measured by EIS obtained for the coil-coated samples during immersion in 0.5 M NaCl solution for the different temperatures.

3.1.2. Water uptake

The water volume fraction variations during immersion in the NaCl solution and for the different temperatures are reported in Fig. 4. It should be emphasized that, due to the presence of the time constant at high frequency, the determination of water uptake in Fig. 4 is limited to 1 h at 60°C, 9 h at 50°C and 65 h at 40°C.

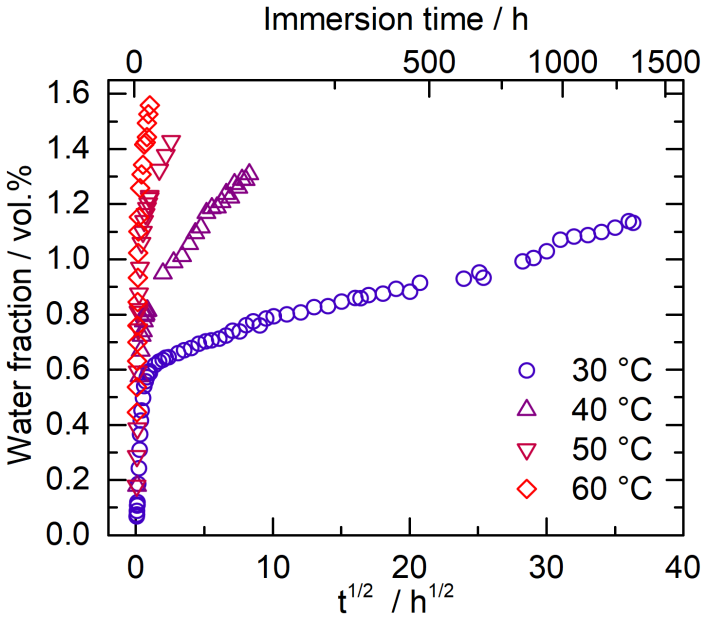

Fig. 4. Water fraction variation of the coil-coated samples as a function of the square root of the immersion time in a 0.5 M NaCl solution for the different temperatures. The determination of water uptake is limited to 1 h at 60°C, 9 h at 50°C and 65 h at 40°C due to the manifestation of the time constant on the impedance diagrams at high frequency.

Fig. 4 shows that the shape of the water uptake curves is similar to that obtained at room temperature with a pseudo-Fickian behaviour which can be decomposed in a Fickian part for short immersion times followed by a slower increase of the water uptake [25]. For 30°C, the water fraction measured at the end of the test (1300 h) is about 1.2 vol.% (close to the value obtained at ambient temperature). From 40°C, the water uptake becomes faster.

To calculate the water diffusion coefficient (D_{water}), the Fickian part of the water uptake was separated from the total water uptake by subtracting the linear increase observed for long immersion times (part II), as shown in Fig. 5 for 40°C. The D_{water} values were calculated according to Eq. 5 [31,32] from the curves reported in Fig. 5b.

$$D_{water} = \frac{P \times l}{\Phi_{\infty}} \times \frac{1}{4}\pi \quad (5)$$

Where P represents the slope of the curve for the initial immersion time, l is the coating thickness (25 µm) and ϕ_{∞} the water uptake at saturation. The values of D_{water} and ϕ_{∞} are reported in Table 2.

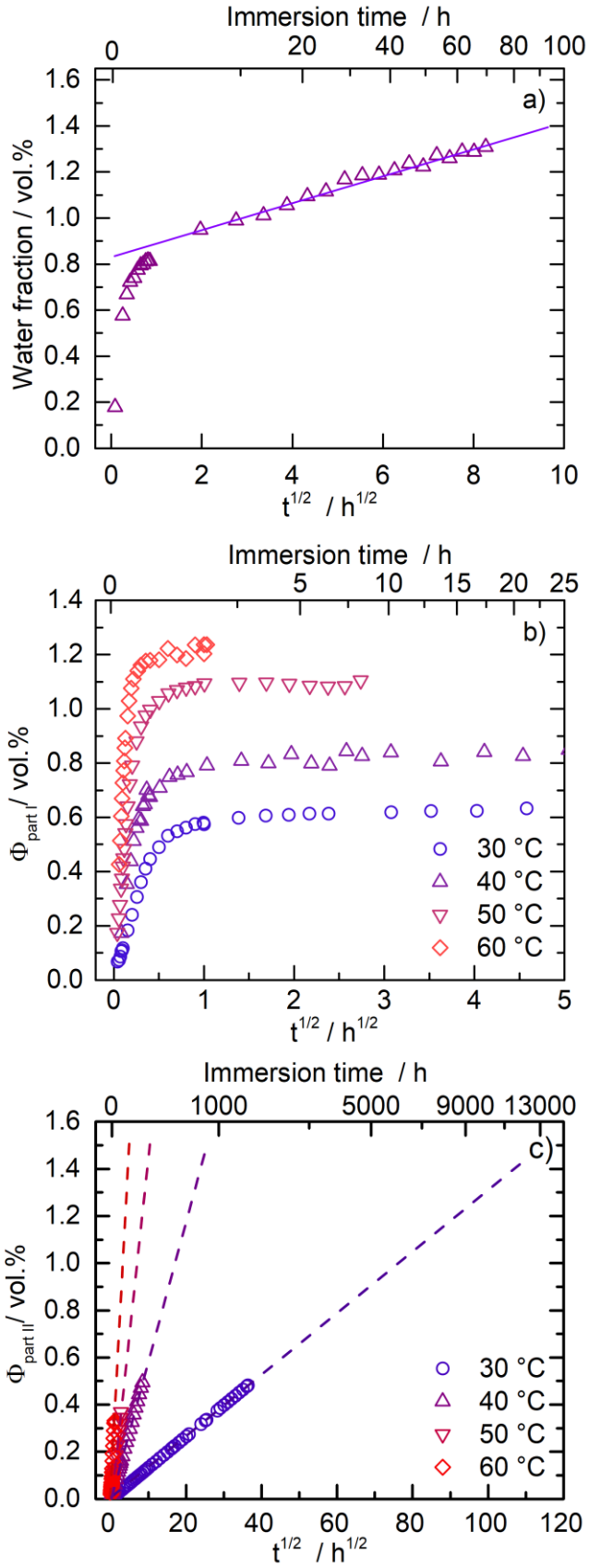

Fig. 5. (a) Example of the water fraction decomposition (40°C) in two different parts; (b) part I: Fickian part of the water uptake for the different temperatures and (c) part II: second part of the water fraction with extrapolations (dotted lines) to reach a water fraction of 1.5 vol.%. The dotted part of the curves will be used in Fig. 6.

Table 2: Water fraction at saturation (ϕ_∞) and diffusion coefficient (D_{water}) for the different temperatures determined from the data in Fig. 5b.

Temperature (°C)	30	40	50	60
ϕ_∞ (%)	0.60 ± 0.05	0.80 ± 0.05	1.10 ± 0. 05	1.25 ± 0.05
D_{water} (10^{12} $m^2.s^{-1}$)	0.8 ± 0.2	1.0 ± 0.2	2.1 ± 0.2	4.9 ± 0.2

Both the water fraction at saturation (ϕ_∞) and the diffusion coefficient (D_{water}) are thermally activated. The D_{water} value at 30°C is in the order of magnitude as those reported in the literature [33,34]. The fast penetration of water into the coating might be linked to diffusion paths suggesting an open and porous coating. This process is exacerbated by the fact that the samples were dried before the EIS experiments. The presence of micro-porosities in the coating would be favourable for water adsorption/desorption phases corresponding in service to immersion and drying phases and also would be necessary for inhibitors release.

The second part of the water uptake contribution is examined in Fig. 5c. It is characterized by a linear behaviour as a function of the square root of the immersion time and thus, it is possible to extrapolate the water uptake for longer immersion times (dotted lines in Fig. 5c), since the values cannot be calculated from the EIS data.

At ambient temperature, similar behaviour has already been observed for polyester coatings and attributed to interactions of the penetrant with the polymer [34]. It can be seen that this second part of water uptake is drastically accelerated by the temperature: similar water uptake after some hours at 60°C corresponds roughly to 1500 h at 30°C. Dotted lines in Fig. 5c indicate that a 1.5 vol.% water fraction would be reached after about 22 h at 60°C and 12700 h at 30°C.

3.1.3. Plasticization

The relaxation times (Fig. 3) were plotted as a function of the water uptake. Only, the second part of the water uptake (Fig. 5c) was considered because it was assumed to be governed by polymer/water interactions, influencing the polymer chain mobility [34,35]. The curves are shown in Fig. 6. When the determination of the water uptake was no longer possible due to the manifestation of the time constant on the impedance diagrams at high frequency, the extrapolated water uptake were used (see dotted lines in Fig. 5c). In Fig. 6, the curves for the different temperatures are almost identical. The two parameters (τ and water uptake) account for the plasticization of the coil-coating. Thus, the superposition of the curves for the four temperatures indicates that, whatever the temperature, the water uptake has a similar impact on the polymer. The plasticization effect is accelerated by the temperature, only.

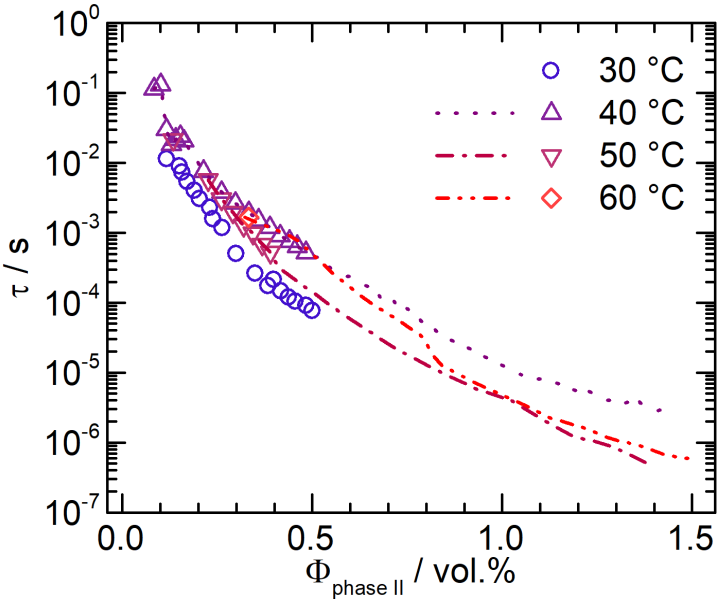

Fig. 6. Time constant as a function of the water fraction (second part) for the different temperatures.

The low but continuous water uptake (without saturation over the studied immersion times) could lead to an accelerated ageing of the coil-coated samples. Indeed, a progressive and continuous water uptake kinetics is favourable to the penetration of aggressive species, such as ions whose penetration kinetics is slower than that of water [9]. In addition, plasticization

indicates that water modifies certain properties of the polymer involved in the initiation or development of blistering (mechanical rigidity, electrical conductivity, ion transport). It appears, from the curves in Fig. 6, that the kinetic of plasticization is strongly accelerated by a rise in temperature, without modification of the involved phenomena. Even though the extrapolations for long immersion times (Fig. 5c and Fig. 6) are approximate, the system reaches a similar aging state after 13000 h (541 days) at 30°C whereas it is a few tens of hours at 60°C which corresponds to the blistering time discussed in the second part of the manuscript.

3.2. Analysis of corrosion / blistering

The second part of the study is dedicated to the detection of corrosion/blistering through the impedance data analysis for the different temperatures. At 60°C, a detailed analysis of the diagrams was performed through the use of electrical equivalent circuits. Typical impedance diagrams obtained at 60°C as a function of the exposure time are shown in Fig. 7. By comparison with those obtained at 40°C (Fig. 2), the diagrams are characterized, from the first days of immersion, by a resistive behaviour at low frequency (constant impedance modulus values). The decrease of the impedance modulus with increasing temperature from 40°C to 60°C can be mainly attributed to the water uptake which results in an increase of both coating conductivity (resistivity decreases at low frequency) and permittivity (capacitive part at high frequency). The rapid decrease of the impedance modulus at low frequency, between 79 and 91 h of immersion (for this sample), might be linked to the corrosion initiation. The repeatability of this phenomenon at 40°C and 60°C was checked for three independent samples. The values of the impedance modulus at 10^{-2} Hz were taken for all the spectra and reported in Fig. 8. For the two temperatures and for short immersion times, the values of the impedance modulus overlap and slightly decrease. The decrease is more pronounced at 60°C due to a higher water uptake which induces an increase of conductivity. The abrupt decrease of the impedance modulus was attributed to the appearance of corrosion and it can be noticed that this

phenomenon presents a rather random character. This random event might be attributed to weak zones in the coating samples facilitating the penetration of aggressive species, particularly Cl^-, triggering the corrosion of the substrate.

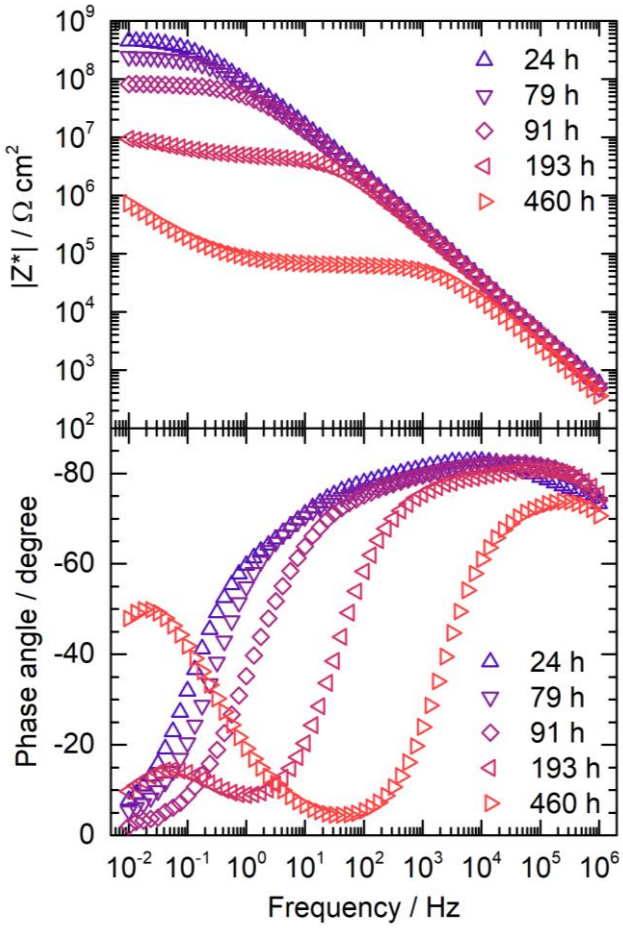

Fig. 7. Impedance diagrams (Bode plots) obtained for the coil-coated sample during immersion in a 0.5 M NaCl solution at 60°C.

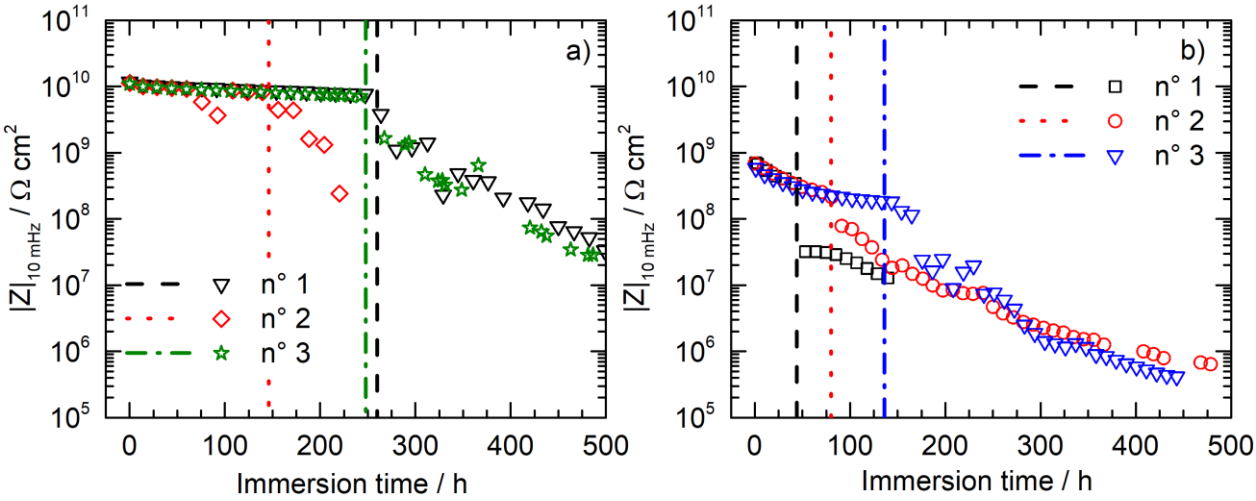

Fig. 8. Impedance modulus at 10^{-2} Hz for the coil-coated samples as a function of immersion time in a 0.5 M NaCl solution at: (a) 40°C and (b) 60°C and for three independent trials. The

vertical lines indicate the time for which an abrupt decrease of the modulus is observed attributed to the corrosion occurrence.

Histogram in Fig. 9 compares the time for which corrosion was detected for the different temperatures. At higher temperatures, the corrosion occurs faster, particularly from 40°C. At 30°C, for the whole period of immersion (more than one month), the samples were undamaged without any deterioration detected from impedance results or visual observations. At 60°C, the corrosion occurs between 44 h and 136 h depending on the samples.

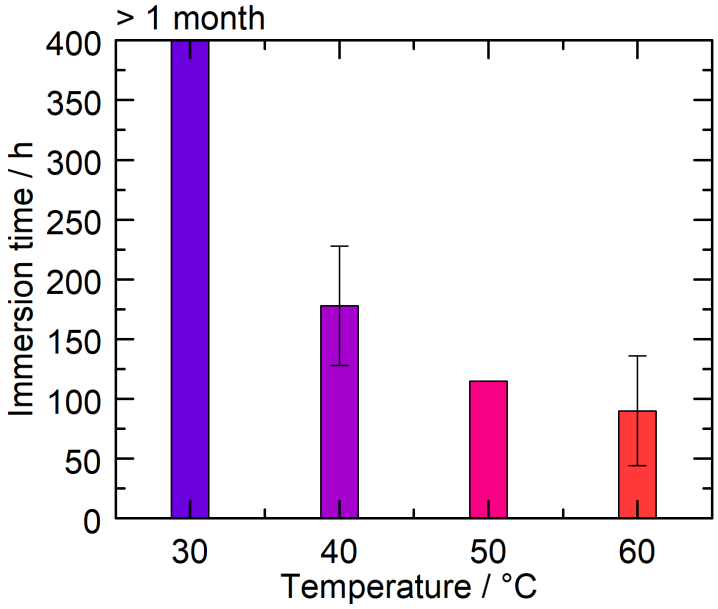

Fig. 9. Immersion time at which corrosion is detected on the impedance spectra for the different temperatures.

The impedance data were analysed by using two equivalent circuits (one for the intact coil-coating and one for the system after corrosion) in order to extract parameters linked to the corrosion process. For the intact coating, it was not possible to use a simple non-ideal RC circuit because the phase angle value, lower than 90 degrees, decreased between 10^5 Hz and 10 Hz, reflecting a "pseudo-CPE" behaviour [36]. Thus, the circuit shown in Fig. 10a was used. The addition of a CPE_x (Q_x and α_x) allows the non-ideal behaviour of the coating capacitance (C_{coat}) to be adjusted as well as the "pseudo-CPE" asymmetry. When the corrosion occured, the diagrams were always characterized by the "pseudo-CPE" at high frequency (Fig. 7). The CPE_x (Q_x and α_x) was thus added to the classical equivalent circuit used to represent defective

coatings (Fig. 10b). The presence of a "pseudo-CPE" on the impedance diagrams might be caused by a distribution of resistivity through the coating [37] linked to heterogeneous zones. These zones would locally have differences in composition and/or reticulation, compared to the rest of the coil-coating. The presence of "weak" zones could explain distributed occurrence of corrosion (Fig. 8). Weak zones in the coating could also be at the origin of local loss of adhesion at the metal/polymer interface which could induce blistering initiation.

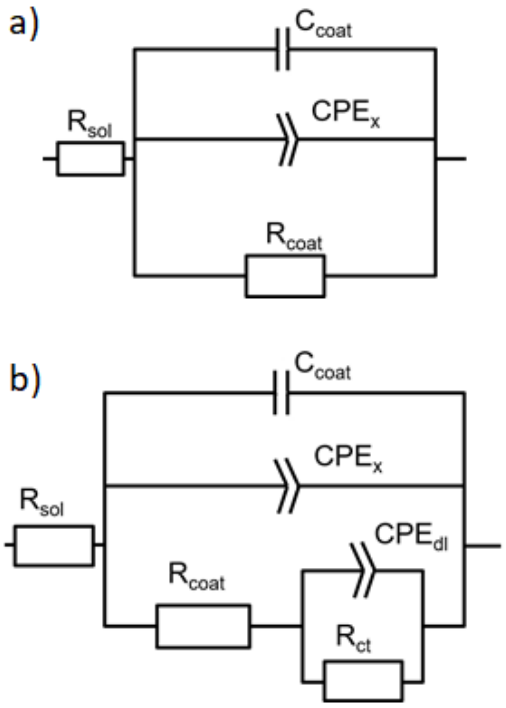

Fig. 10. Equivalent electrical circuits used to fit the impedance data: (a) intact coating and (b) after corrosion. R_{sol}, R_{coat} and R_{ct} represent the electrolyte resistance, the coating resistance and the charge transfer resistance, respectively; C_{coat} represents the coating capacitance; CPE_{dl} is the constant phase element associated with the double layer on the metal substrate with the parameters Q_{dl} and α_{dl}. CPE_x is introduced to account for a pseudo-CPE behaviour (with the parameters Q_x and α_x).

Three examples of experimental and fitted data are shown in Fig. 11. A good agreement is observed. The parameters associated with the coating (R_{coat} and C_{coat}) are not discussed afterwards. The time constant associated with the corrosion process was analysed from the parameters R_{ct}, Q_{dl} and α_{dl}. Some values obtained from the fitting procedure are reported in

Table 3. When the immersion time increased, the R_{ct} values decreased rapidly whereas the Q_{dl} values significantly increase and the α_{dl} values increased from 0.7 to 0.8.

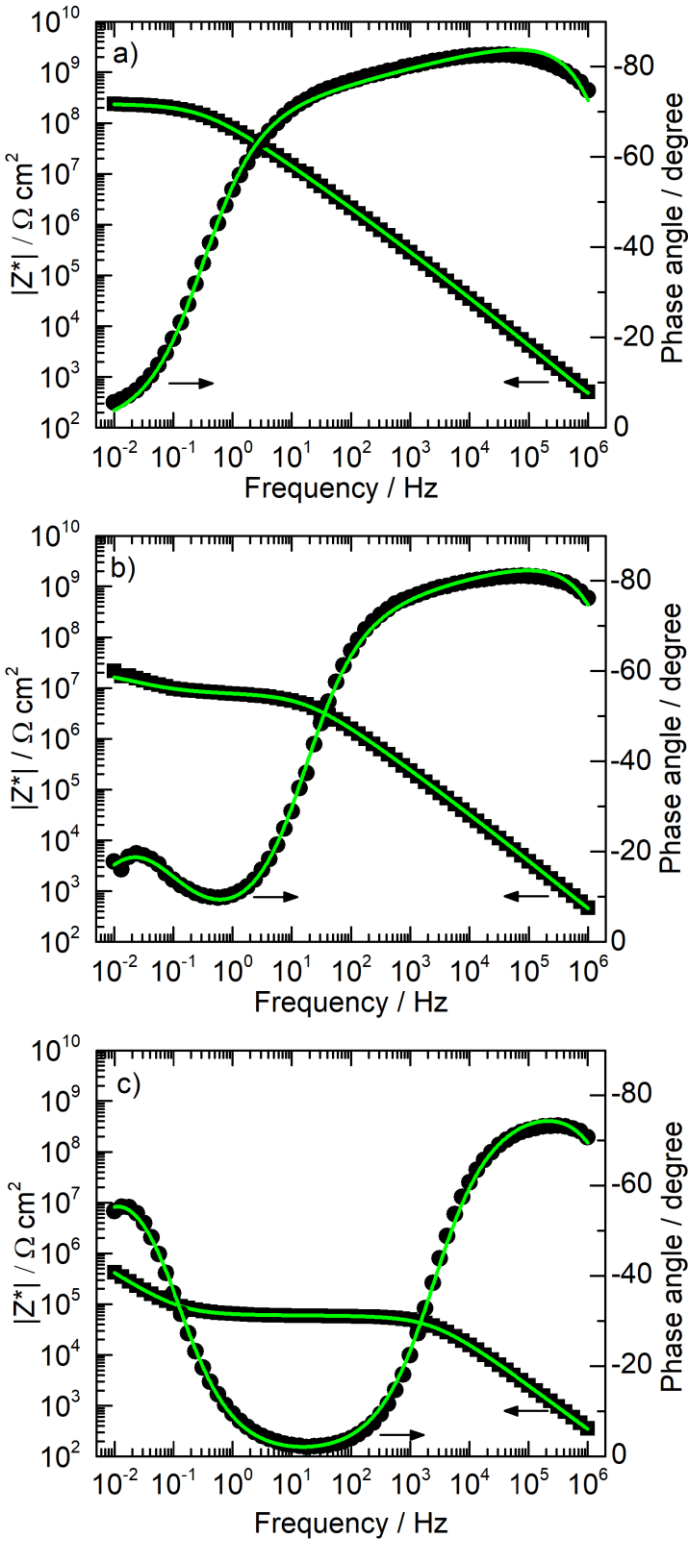

Fig. 11. Examples of the experimental data and the adjusted diagrams with the equivalent circuits shown in Fig. 10 for three immersion time (For this sample, corrosion appears after 136 h of immersion): (a) 73 h (intact coating); (b) 217 h (81 h after the appearance of corrosion) and (c) 434 h (298 h after the appearance of corrosion).

Table 3: R_{ct}, Q_{dl}, *and* α_{dl} values as a function of the immersion time after corrosion appearance in a 0.5 M NaCl solution at 60°C for the coil-coated sample.

Immersion time after corrosion appearance (h)	72	120	144	168	193	216	240	289	304	484
R_{ct} (Ω cm^2)	16.0 10^6	5.8 10^6	2.7 10^6	1.9 10^6	2.0 10^6	3.3 10^6	2.8 10^6	2.3 10^6	2.2 10^6	1.8 10^6
Q_{dl} (Ω^{-1} cm^2 s$^{\alpha}$)	4.4 10^{-7}	1.3 10^{-6}	3.1 10^{-6}	5.8 10^{-6}	7.8 10^{-6}	1.0 10^{-5}	1.3 10^{-5}	2.2 10^{-5}	2.5 10^{-5}	3.9 10^{-5}
α_{dl}	0.69	0.70	0.75	0.76	0.79	0.79	0.79	0.80	0.80	0.81

Capacitance values (C_{dl}) were calculated from the CPE parameters (Q_{dl} and α_{dl}) considering a 2D distribution of the charge transfer resistances on the electrode surface, by using the Brug formula [38].

$$C_{dl} = {Q_{dl}}^{\frac{1}{\alpha_{dl}}} \times \left(\frac{1}{R_e} + \frac{1}{R_{ct}}\right)^{\frac{\alpha_{dl}-1}{\alpha_{dl}}} \quad (6)$$

From these data, it was possible to analyse the C_{dl} variation *vs* the exposure time to the electrolyte whereas this was not possible with the Q_{dl} values which are closely associated with the α_{dl} parameter. From a corrosion point of view, the C_{dl} value is linked to the active surface area, S_{active}, which can be estimated from Eq. 7:

$$S_{active} = \frac{C_{dl}}{C_{zinc}} \times A \quad (7)$$

C_{zinc} is the double layer capacitance of a bare zinc surface, measured in the same electrolyte and A is the exposed surface area (14.6 cm^2). In the literature, C_{zinc} value varies between 50 and 500 µF cm^{-2} [39–41]. These threshold values, used to calculate S_{active}, lead to error bars reported in Fig. 12. Shortly after the corrosion appearance (abrupt decrease of the impedance modulus), it was not possible to extract the corroded surface area from the impedance data (the low frequency time constant was not visible). Thus, the first estimate of the corroded surface

area by the impedance fitting is 0.01 cm^2 (73 h after the corrosion initiation). This value increases to 10 cm^2 after 480 h. A linear extrapolation of the first points at t = 0 (Fig. 12) gives a corroded surface area of about 0.02 mm^2 (corroded zone or blister of 80 µm in diameter). This surface area would correspond, for the studied sample, to the limit of detection of a corrosion defect by EIS.

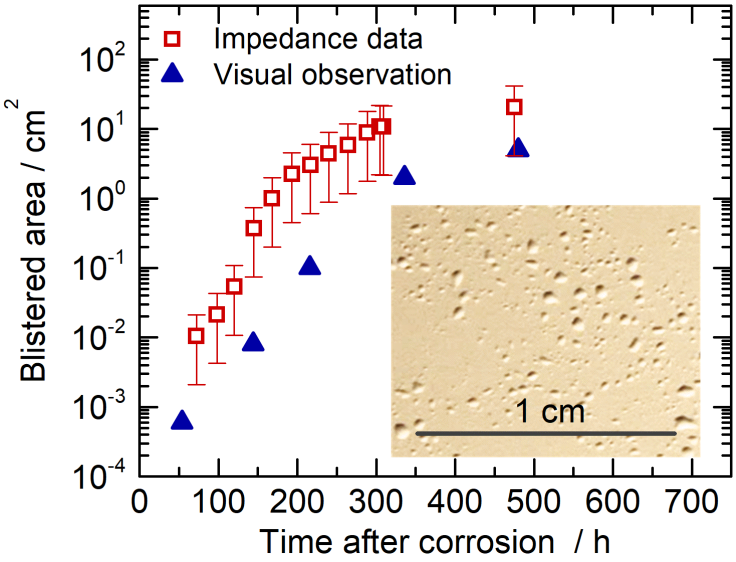

Fig. 12. Variation and comparison of the corroded and blisters surface areas determined from the impedance data and from the images analysis as a function of the immersion time (after the appearance of corrosion) in the NaCl solution at 60°C. Error bars on the impedance data correspond to the uncertainty on the C_{dl} value for the bare zinc surface (50 to 500 µF.cm^{-2}). Insert: image of the coil-coating sample after 450 h of immersion in a 0.5 M NaCl solution at 60°C.

The surface areas calculated from the impedance data were compared with visual observations. The sample, characterized by EIS, was removed from the immersion at regular time intervals to observe the surface. Fig. 12 (insert) shows the surface of the coil-coating sample at the end of the experiment (620 h of immersion at 60°C). The image reveals blisters with different sizes all over the surface (generalized blistering). In Fig. 12, the blisters surface areas measured by visual observation are compared with the corroded surface areas determined from the EIS data analysis. The surface areas are significantly higher when they are measured by EIS (around 10 times higher) but the variation is quite similar. This difference could be explained by the C_{dl} values calculated from the CPE parameters thanks to the Brug formula.

The surface areas measured by the image analysis account only for the blisters but corrosion could also occur near the blister, below the coating (cathodic zones). This would lead to an underestimation of the total blister areas. Moreover, blisters smaller than the detection limit, imposed by the surface roughness and topology cannot be detected and are not considered.

4. Conclusions

Impedance characterization of a commercial coil-coating was carried out at different temperatures. Measurement protocol was optimized to determine water uptake for very short immersion times (some minutes). In the initial step, a fast water uptake was shown. This behaviour is characteristic of coating with “micro-pores” which allows controlled exchanges of a small amount of water through the coating. This reversibility regarding water uptake is necessary to avoid water accumulation at the metal/coating interface, particularly in service during immersion and drying phases. For longer immersion times, slower and continuous water uptake was observed. It reveals plasticization of the polymer matrix (interactions between water molecules and the organic coating).

The acceleration of plasticization was demonstrated through an increase of the applied temperature, leading to an increase in the water uptake and a decrease of the relaxation time associated with the dielectric manifestation of the glass transition. The ageing of coil-coatings was found significantly accelerated from 40°C isothermal experiment, which resulted in blistering events within moderate delays. Detection of blistering was correlated to corrosion phenomena and detected on EIS diagrams through a sharp decrease in the low frequency modulus. Blistered surface areas calculated from the impedance data by using an electrical equivalent circuit were found to be in good agreement with those determined from optical techniques. These similar results demonstrate a direct relationship between corrosion and blistering, yet without an indication as to whether corrosion is a cause or consequence of blistering. One innovative character of this work lies in the use of thermally enhanced EIS to

monitor ageing of materials as a function of immersion temperature, including the appearance and surface characterization of blistering events.

References

[1] K. Pélissier, N. Le Bozec, D. Thierry, N. Larché, Evaluation of the long-term performance of marine and offshore coatings system exposed on a traditional stationary site and an operating ship and its correlation to accelerated test, Coatings. (2022). https://doi.org/10.3390/coatings12111758.

[2] H.J. Tiemens, M. Hoeflaak, The performance level of some commercial coil-coated materials, Constr. Build. Mater. 8 (1994) 243–259. https://doi.org/10.1016/S0950-0618(09)90008-3.

[3] H. Leidheiser, W. Funke, Water disbondment and wet adhesion of organic coatings on metals: a review and interpretation, J. Oil Colour Chem. Assoc. 70 (1987) 121–132. http://lib3.dss.go.th/fulltext/scan_ebook/j_of_oil_chem_1987_v70_n5.pdf.

[4] W. Funke, Blistering of paint films and filiform corrosion, Prog. Org. Coatings. 9 (1981) 29–46. https://doi.org/10.1016/0033-0655(81)80014-3.

[5] C.H. Hare, Blistering of paint films on metal, Part 1: osmotic blistering, J. Prot. Coatings Linings. 15 (1998) 45–63.

[6] H. Leidheiser, R.D. Granata, Ion transport through protective polymeric coatings exposed to an aqueous phase, IBM J. Res. Dev. 32 (1988) 582–590. https://doi.org/10.1147/RD.325.0582.

[7] O. Negele, W. Funke, Internal stress and wet adhesion of organic coatings, Prog. Org. Coatings. 28 (1996) 285–289. https://doi.org/10.1016/0300-9440(95)00606-0.

[8] E.D. Schachinger, R. Braidt, B. Strauß, A.W. Hassel, EIS study of blister formation on coated galvanised steel in oxidising alkaline solutions, Corros. Sci. 96 (2015) 6–13. https://doi.org/10.1016/J.CORSCI.2014.12.010.

[9] N. Madelat, B. Wouters, E. Jalilian, G. Van Assche, A. Hubin, H. Terryn, T. Hauffman, Differentiating between the diffusion of water and ions from aqueous electrolytes in organic coatings using an integrated spectro-electrochemical technique,

Corros. Sci. 212 (2023) 110919. https://doi.org/10.1016/J.CORSCI.2022.110919.

[10] M. Hoseinpoor, T. Prošek, J. Mallégol, Novel approach to measure water vapor permeability in pre-painted metals using adapted cup method: Correlation between permeation rate and tendency to blistering, Prog. Org. Coatings. 169 (2022) 106917. https://doi.org/10.1016/J.PORGCOAT.2022.106917.

[11] F. Deflorian, L. Fedrizzi, S. Rossi, P.L. Bonora, Organic coating capacitance measurement by EIS: ideal and actual trends, Electrochim. Acta. 44 (1999) 4243–4249. https://doi.org/10.1016/S0013-4686(99)00139-5.

[12] G.P. Bierwagen, L. He, J. Li, L. Ellingson, D.E. Tallman, Studies of a new accelerated evaluation method for coating corrosion resistance — thermal cycling testing, Prog. Org. Coatings. 39 (2000) 67–78. https://doi.org/10.1016/S0300-9440(00)00106-5.

[13] B.R. Hinderliter, S.G. Croll, D.E. Tallman, Q. Su, G.P. Bierwagen, Interpretation of EIS data from accelerated exposure of coated metals based on modeling of coating physical properties, Electrochim. Acta. 51 (2006) 4505–4515. https://doi.org/10.1016/J.ELECTACTA.2005.12.047.

[14] D.M. Brasher, A.H. Kingsbury, Electrical measurements in the study of immersed paint coatings on metal. I. Comparison between capacitance and gravimetric methods of estimating water-uptake, J. Appl. Chem. 4 (1954) 62–72. https://doi.org/10.1002/JCTB.5010040202.

[15] A.S. Castela, A.M. Simões, Assessment of water uptake in coil coatings by capacitance measurements, Prog. Org. Coatings. 46 (2003) 55–61. https://doi.org/10.1016/S0300-9440(02)00190-X.

[16] C. Vosgien Lacombre, G. Bouvet, D. Trinh, S. Mallarino, S. Touzain, Water uptake in free films and coatings using the Brasher and Kingsbury equation: a possible explanation of the different values obtained by electrochemical Impedance spectroscopy and gravimetry, Electrochim. Acta. 231 (2017) 162–170.

https://doi.org/10.1016/J.ELECTACTA.2017.02.051.

[17] A.S. Nguyen, N. Causse, M. Musiani, M.E. Orazem, N. Pébère, B. Tribollet, V. Vivier, Determination of water uptake in organic coatings deposited on 2024 aluminium alloy: Comparison between impedance measurements and gravimetry, Prog. Org. Coatings. 112 (2017) 93–100. https://doi.org/10.1016/J.PORGCOAT.2017.07.004.

[18] M. Hoseinpoor, T. Prošek, L. Babusiaux, J. Mallégol, Simplified approach to assess water uptake in protective organic coatings by parallel plate capacitor method, Mater. Today Commun. 26 (2021) 101858. https://doi.org/10.1016/J.MTCOMM.2020.101858.

[19] I.C.P. Margarit-Mattos, EIS and organic coatings performance: Revisiting some key points, Electrochim. Acta. 354 (2020) 136725. https://doi.org/10.1016/J.ELECTACTA.2020.136725.

[20] H. Ochs, J. Vogelsang, Effect of temperature cycles on impedance spectra of barrier coatings under immersion conditions, Electrochim. Acta. 49 (2004) 2973–2980. https://doi.org/10.1016/J.ELECTACTA.2004.01.056.

[21] L. Valentinelli, J. Vogelsang, H. Ochs, L. Fedrizzi, Evaluation of barrier coatings by cycling testing, Prog. Org. Coatings. 45 (2002) 405–413. https://doi.org/10.1016/S0300-9440(02)00137-6.

[22] Z. Sharer, J. Sykes, Insights into protection mechanisms of organic coatings from thermal testing with EIS, Prog. Org. Coatings. 74 (2012) 405–409. https://doi.org/10.1016/J.PORGCOAT.2011.12.002.

[23] Z. Sharer Sahir, J.M. Sykes, Effect of temperature on the impedance response of coated metals, Prog. Org. Coatings. 77 (2014) 2039–2044. https://doi.org/10.1016/J.PORGCOAT.2014.02.009.

[24] J.M. Sykes, E.P. Whyte, X. Yu, Z. Sharer Sahir, Does “coating resistance” control corrosion?, Prog. Org. Coatings. 102 (2017) 82–87.

https://doi.org/10.1016/J.PORGCOAT.2016.04.015.

[25] P. Bonin, A. Roggero, N. Caussé, N. Pébère, D. Thierry, N. Le Bozec, Impedance analysis of the barrier effect of coil-coated materials: Water uptake and glass transition variations, Prog. Org. Coatings. 153 (2021) 106163. https://doi.org/10.1016/J.PORGCOAT.2021.106163.

[26] M. Bakalli, P. Keil, W. Strunz, T. Broeker, R. Herrmann, J. Vogelsang, Critical view of the results of the 2nd international round-robin test on EIS measurements of organic coatings, Prog. Org. Coatings. 180 (2023) 107565. https://doi.org/10.1016/J.PORGCOAT.2023.107565.

[27] C.G. Malmberg, A.A. Maryott, Dielectric constant of water from 0 to 100 C, J. Res. Natl. Bur. Stand. (1934). 56 (1956) 1. https://doi.org/10.6028/jres.056.001.

[28] F. Kremer, A. Schönhals, Broadband dielectric spectroscopy, Springer Science & Business Media, 2002.

[29] A. Roggero, L. Villareal, N. Caussé, A. Santos, N. Pébère, Correlation between the physical structure of a commercially formulated epoxy paint and its electrochemical impedance response, Prog. Org. Coatings. 146 (2020) 105729. https://doi.org/10.1016/J.PORGCOAT.2020.105729.

[30] G.M. Foster, S. Ritchie, K.E. Evans, C. Lowe, Controlled relative humidity testing for the characterisation of the brittle-tough and glass transition temperatures of coil coating paint films, Prog. Org. Coatings. 51 (2004) 244–249. https://doi.org/10.1016/J.PORGCOAT.2004.08.002.

[31] J. Crank, Diffusion in a plane sheet, in: Math. Diffus., Oxford University Press, London, 1975: pp. 47–48.

[32] F. Bellucci, L. Nicodemo, Water transport in organic coatings, Corrosion. 49 (1993) 235–247. https://doi.org/10.5006/1.3316044.

[33] T. Prosek, A. Nazarov, J. Stoulil, D. Thierry, Evaluation of the tendency of coil-coated

materials to blistering: Field exposure, accelerated tests and electrochemical measurements, Corros. Sci. 61 (2012) 92–100. https://doi.org/10.1016/J.CORSCI.2012.04.026.

[34] E.D. Schachinger, B. Strauß, R. Braidt, A.W. Hassel, Electrochemical impedance spectroscopy on UV-aged polyester Coatings: possibilities and limits of modeling water diffusion, Phys. Status Solidi. 217 (2020) 1901038. https://doi.org/10.1002/PSSA.201901038.

[35] G.W. Walter, The application of impedance methods to study the effects of water uptake and chloride ion concentration on the degradation of paint films—II. Free films and attached/free film comparisons, Corros. Sci. 32 (1991) 1085–1103. https://doi.org/10.1016/0010-938X(91)90095-7.

[36] A.S. Nguyen, M. Musiani, M.E. Orazem, N. Pébère, B. Tribollet, V. Vivier, Impedance analysis of the distributed resistivity of coatings in dry and wet conditions, Electrochim. Acta. 179 (2015) 452–459. https://doi.org/10.1016/J.ELECTACTA.2015.02.109.

[37] B. Hirschorn, M.E. Orazem, B. Tribollet, V. Vivier, I. Frateur, M. Musiani, Constant-phase-element behavior caused by resistivity distributions in films: I. Theory, J. Electrochem. Soc. 157 (2010) C452. https://doi.org/10.1149/1.3499564.

[38] G.J. Brug, A.L.G. van den Eeden, M. Sluyters-Rehbach, J.H. Sluyters, The analysis of electrode impedances complicated by the presence of a constant phase element, J. Electroanal. Chem. 176 (1984) 275–295. https://doi.org/10.1016/S0022-0728(84)80324-1.

[39] M. Keddam, A. Hugot-Le-Goff, H. Takenouti, D. Thierry, M.C. Arevalo, The influence of a thin electrolyte layer on the corrosion process of zinc in chloride-containing solutions, Corros. Sci. 33 (1992) 1243–1252. https://doi.org/10.1016/0010-938X(92)90133-N.

[40] C. Pérez, A. Collazo, M. Izquierdo, P. Merino, X.R. Nóvoa, Electrochemical impedance spectroscopy study of the corrosion process on coated galvanized steel in a salt spray fog chamber, Corrosion. 56 (2000).

[41] S. He, H. Zhong, EIS study of corrosion behavior of hot-dip galvanized steel in 5% NaCl aqueous solution, Adv. Mater. Res. 335–336 (2011) 779–782. https://doi.org/10.4028/WWW.SCIENTIFIC.NET/AMR.335-336.779.